Progress In Electromagnetics Research C, Vol. 164, 186–194, 2026

PIER C

(Received 14 November 2025, Accepted 11 December 2025, Scheduled 9 January 2026)

Design and Performance Evaluation of a Narrow-Band Metasurface Radomes for Reduction of RCS in Stealth Applications

Pandigunta A. Kumari[1], Madhavareddy V. Narayana[1], Govardhani Immadi[1,*], Yogesh Solunke[2], and Kanaparthi V. Phani Kumar[3]

[1]*Department of Electronics and Communication Engineering, KLEF, Vaddeswaram, Guntur, Andhra Pradesh, India*
[2]*Department of Electronics and Communication Engineering, VNIT NAGPUR, India*
[3]*Department of Electronics and Communication Engineering, School of Engineering and Applied Sciences SRM University-AP, Neerukonda, Andhra Pradesh-522240, India*

ABSTRACT: A compact metasurface absorber based on a novel combination of concentric split-ring resonators (SRRs) and arc dipoles is presented in this work. The proposed CSAD-based absorber with a copper structure consists of quad dipoles and SRRs with a dielectric constant of 4.3 and loss tangent of 0.02. The design resonates near the frequency of 17 GHz with a bandwidth of 300 MHz and 99.9% absorption. The symmetric single-band metasurface allows for polarization-independent, angle-stable absorption up to 60°. The unit cell size for the proposed design is $10.375 \times 10.375 \times 1.6\,\text{mm}^3$. It can be used for reducing the radar cross-section for stealth applications, such as UAVs that require selective frequency absorption. Simulations closely match observations, verifying the metasurface's high stability and demonstrating its usefulness for practical electromagnetic validations.

1. INTRODUCTION

Metamaterials are periodically arranged materials having subwavelength structures designed to manipulate electromagnetic waves, which are artificially engineered structures, not naturally occurring materials. The generation and manipulation of electromagnetic waves are employed using radio frequency (RF) components, such as low noise amplifiers (LNAs) [1], antennas, power amplifiers, and metasurfaces. In contrast, metasurfaces are essentially two-dimensional counterparts of metamaterials; they offer a simpler and highly efficient approach for electromagnetic devices [2]. Recent wearable metasurface improvements have been made in simpler, lightweight, and easily made designs to improve performance. Thin, flexible metasurfaces precisely regulate electromagnetic waves for antennas, cloaking, and imaging, allowing for dynamic waveguiding, beam steering, and sophisticated beam shaping [3–5]. Metasurfaces can provide polarisation conversion and stealth at 17 GHz. A 22×22 array controls an electromagnetic wave for sensors and antennas in microwave to optical ranges with frequencies of 7.1–8 GHz and 13.3–25.8 GHz [6]. Recent metasurface designs efficiently adjust terahertz wave polarization from 2.04 to 5.33 THz with 89% bandwidth, over 90% polarization conversion ratio (PCR), and a 10 dB reduction in radar cross-section (RCS), allowing for enhanced wave control and modelling in stealth and electromagnetic (EM) applications [7, 8]. A compact metasurface antenna with square split-ring and U-shaped elements operates at 3.5 GHz with dual beams at $\pm 45°$ and reflection below -10 dB, improving 5G Pico cell performance with high capacity and low interference [9]. Dartboard metasurfaces use polarization conversion unit cells to create orbital angular momentum while reducing RCS. With over 10 dB RCS reduction (RCSR) from 4 to 17.1 GHz, they improve stealth by reducing radar visibility without impacting antenna performance, which is critical for advanced aircraft and defence applications [10, 11]. An ultra-wideband metasurface absorber is proposed to achieve over 90% absorptance from 5.5 to 36.56 GHz with angular stability up to 40°. Fabricated arrays demonstrate performance in the X-, Ku-, and K-bands, enabling superlensing, polarisation control, and RCS reduction [12, 13]. A compact, ultra-thin metasurface enhances ultra-high frequency (UHF) radio frequency identification (RFID) performance by reducing reflections and boosting gain. It achieves $> 99\%$ absorption at 9.35, 15.21, and 19.76 GHz, dual-band polarisation conversion (14.6–26.8 GHz, 31–33.5 GHz), and stable PCR > 0.9 up to 50° incidence [14–16]. Metasurfaces reduce RCS by up to 17.2 dB across 11–17 GHz, offering lightweight, easily fabricated solutions for stealth and aerospace applications. Future research targets reconfigurable metasurfaces for adaptive electromagnetic wave control [17–19]. A unique golden-frequency selective surface (G-FSS) with closely spaced dual-band-stop features provides adequate shielding for C- and X-band applications. Its golden fractal-based design, paired with symmetrical construction, provides outstanding angular stability, minimal

* Corresponding author: Govardhani Immadi (govardhanee_ec@kluniversity.in).

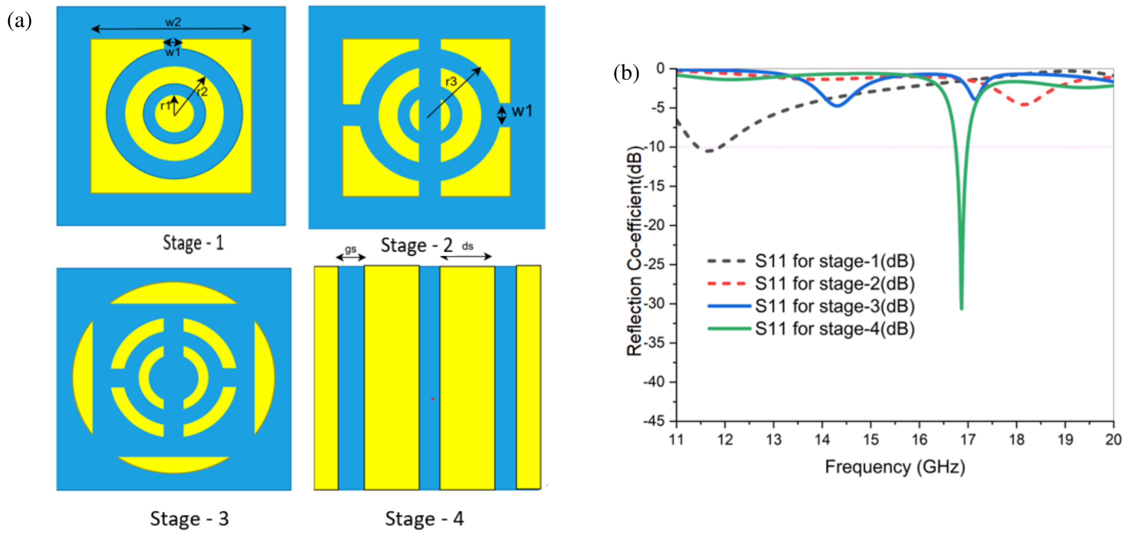

FIGURE 1. (a) Analysis of the proposed CSAD unit cell in stages. (b) Reflection coefficient for stages 1, 2, 3, and final design.

RCS, and adaptation to conformal surfaces, making it particularly ideal for military applications [20].

In this work, a metasurface based on a novel combination of concentric split ring resonators (SRRs) and arc dipoles is presented. It consists of quad arc dipoles and SRRs with a dielectric constant of 4.3 and loss tangent of 0.02. The symmetric single-band metasurface size is $10.375 \times 10.375 \times 1.6\,\text{mm}^3$. It resonates near the frequency 17 GHz and consists of bandwidth 300 MHz. The Concentric-SRR Arc-Dipole (CSAD) based metasurface shows an absorption of 99.9% and demonstrates polarization-independent and angle with a stable absorption up to 60°. Due to these characteristics, it is suitable for stealth applications.

Following the introduction, Section 2 represents a detailed theoretical and structural description of the CSAD metasurface, including its geometric configuration and electromagnetic operating mechanism. Section 3 investigates the array analysis of the unit cell, with dedicated subsections examining 2×2 and 4×4 finite array configurations to validate periodicity and mutual coupling effects. Section 4 describes the absorption characteristics of CSAD structure. Section 5 discusses a comprehensive parametric analysis by varying key geometrical parameters to evaluate their influence on performance. Section 6 examines the angular stability of the metasurface up to 60° oblique angle of incidence for TE and TM polarizations. Section 7 analyzes the E-field distribution and surface current distributions to investigate the absorption mechanism. Section 8 demonstrates the RCS reduction capability. Section 9 compares the proposed metasurface with previously reported designs to highlight its relative advantages. Finally, the paper is concluded with Section 10.

2. ANALYSIS OF CSAD UNIT CELL

The design analysis of the proposed CSAD is illustrated in Figure 1. Introducing from Stage 1, the unit cell is designed with two split rings [21], which form an LC resonator with inductance from the current loop and capacitance from the narrow gaps. Although a high electric field occurs within the gaps, limited free-space coupling results in poor impedance matching, providing a narrow resonance with S_{11} below 10 dB at 17 GHz. In Stage-2, the central metallic strip increases inductive loading and strengthens near-field electric-magnetic coupling with the split-ring resonator [22], slightly shifting the resonant frequency upward and improving impedance matching. However, the achieved reflection coefficient remains limited to around -12 dB. In Stage-3, after several design iterations, a unit cell combining concentric split-rings, a conductive strip, and arc-dipole elements [23] is introduced to enhance capacitive–inductive coupling. This coupling configuration improves impedance matching approximately equal to free space, and the periodic conductive strip array exhibits distributed LC behaviour, but with poor selectivity and an absence of a distinct S_{11} resonance. In Stage-4, by introducing 1 mm wide slots in the ground plane with a copper layer, the periodic strip array exhibits distributed LC behaviour characteristics, and the performance is significantly improved. The final design achieved an S_{11} of -33 dB at 17 GHz, illustrated in Figure 1.

The design of the CSAD unit cell is shown in Figure 2. The Concentric-SRR Arc-Dipoles (CSADs) combine a dual-split-ring resonator (SSR) and four curved dipole-like arc excite magnetic and electric resonances. It features two crossed dipoles combined with a symmetric circular Split Ring Resonator (SRR). Additionally, semi-circular metallic sheets are integrated onto a substrate, with a dielectric constant of 4.3, which has the width of 1.6 mm. A ground plane is included on the back to the substrate to establish a uniform electric field and minimize transmission losses. This ground plane is made up of copper with a thickness of 0.035 mm.

The unit cell structure incorporates dual circular ring resonators along with parallel copper plates. The overall dimensions of the unit cell design are shown in Table 1.

This structural configuration is optimized for effective electromagnetic performance at 17 GHz frequency.

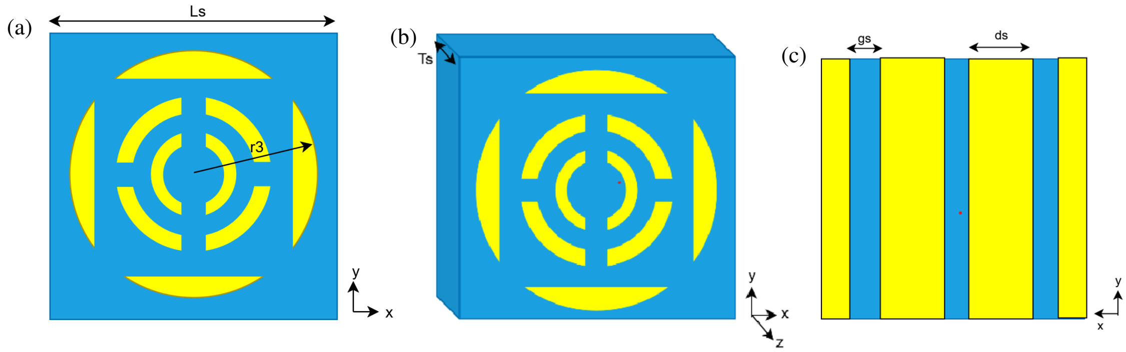

FIGURE 2. The proposed CSAD design, (a) front view, (b) prospective view, and (c) back view.

TABLE 1. The dimensions of the proposed design.

Factor	Value (mm)	Factor	Value (mm)
L_s	10.375	r_3	5
w_1	0.5	T_s	1.6
w_2	0.6	g	1
r_1	1.5	g_s	1
r_2	3.5	d_s	2.5

By simulating, the proposed unit cell comprising CSAD in Computer Simulation Technology (CST) Studio, various key parameters were analyzed, including return loss, parametric analysis of w, TE and TM modes, Absorption, RCS reduction, and effective permeability. The unit cell is modelled with periodic boundary conditions and waveguide ports to accurately represent electromagnetic behavior. A higher return loss (more negative dB value) indicates lower reflection and improves impedance matching, while values closer to 0 dB imply poor matching and greater reflection. The simulated and measured results are realized in Ku-band (12 GHz–18 GHz) of frequency according to boundary conditions, shown in Figure 3.

2.1. Robust Retrieval Method

To obtain the effective permittivity and permeability of a metamaterial, the structure is modeled as an equivalent homogeneous medium. Under this assumption, the effective parameters can be extracted using reflection S_{11} and transmission S_{21} coefficients. For EM wave incident normally on a homogeneous of thickness L_s, with the coordinate origin located at the first interface of the slab, S_{11} corresponds to the reflection coefficient. The transmission coefficient T is related to S_{21} through the relation [24]

$$S_{21} = Te^{ik_0 d}$$

k_0 denotes the free-space wavenumber to incident wave. The retrieved S-parameters can be used to determine refractive index n and impedance Z of the metamaterial, as described in [25–27].

$$S_{11} = \frac{R_{01}\left(1 - e^{ink_o d}\right)}{1 - R_{01}^2 e^{ink_o d}} \tag{1}$$

$$S_{21} = \frac{\left(1 - R_{01}^2\right) e^{ink_o d})}{1 - R_{01}^2 e^{ink_o d}} \tag{2}$$

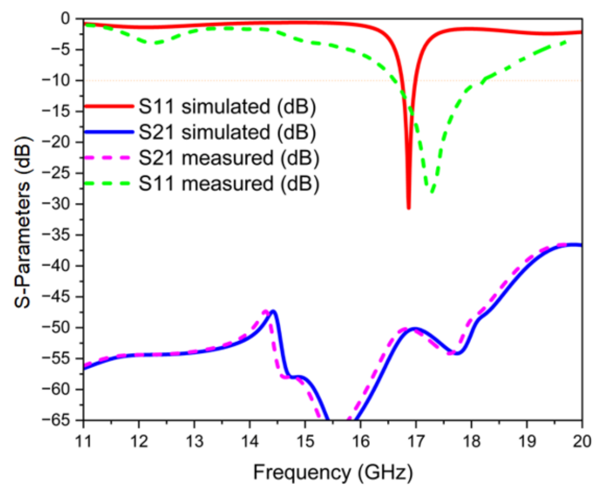

FIGURE 3. Frequency response for proposed design (S_{11}).

where $R_{01} = \frac{1+Z}{1-Z}$.

For CSAD metasurface absorbers, the ground plane reduces wave transmission, making the transmission coefficient negligible. The EM response of metasurface can be determined using the surface impedance, Zsurface [28]. As mentioned, the refractive index and impedance matching can be obtained from the above equations as

$$Zsurface = \pm\sqrt{\frac{\left(l + s_{11}\right)^2 - S_{21}^2}{\left(1 - s_{11}\right)^2 - S_{21}^2}} \tag{3}$$

$$n = \frac{1}{k_0 d}\left\{\left[\left[\ln\left(e^{ink_o d}\right)\right]'' + 2m\pi\right] - \mathrm{i}\cdot\left[\ln\left(e^{ink_o d}\right)\right\}\right. \tag{4}$$

The permittivity and permeability can be measured using (3) and (4). The above relation derives EM boundary conditions that interface between free space (Z_0) [28] and an impedance surface, which shows impedance matching behaviour of the metasurface. The CSAD metasurface is backed with a ground plane, and then the effective permeability can be approximated using

$$Permittivity\ \varepsilon = \frac{n}{z} \tag{5}$$

$$Permeability\ \mu = n \cdot Z \tag{6}$$

Relative permeability is a material that defines how a medium reacts to a magnetic field in relation to space (Z_0). It is essential for manipulating electromagnetic waves, particularly on constructed surfaces such as metasurfaces. Metasurfaces are meant to alter a surface's electric and magnetic reactions to control wave behaviour such as reflection, transmission, and polarisation. Negative permeability at Ku band of frequencies leads to a negative refractive index, backwards wave propagation as shown in Figure 4.

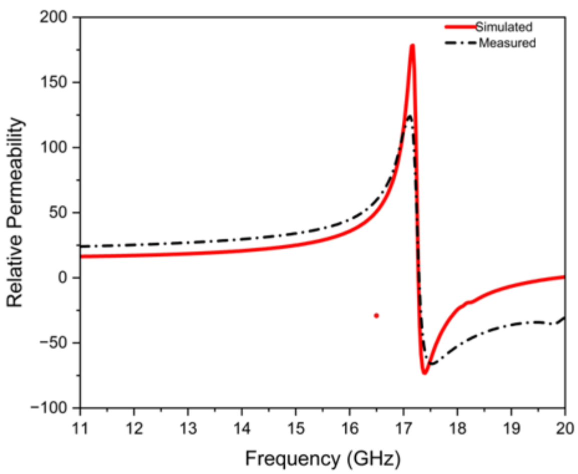

FIGURE 4. Relative permeability.

3. ARRAY ANALYSIS OF CSAD

3.1. 2×2 CSAD Metasurface

A single unit cell is idealized and assumes infinite periodicity because of periodic boundary conditions. In practical implementations, finite arrays (e.g., 10×10 or 20×20) and even 2×2 provide a closer approximation of how genuine metasurfaces operate.

Now the proposed unit cell is arranged in a $2 * 2$ array of unit cells, which acts as a metasurface. By simulating the proposed 2×2 metasurface unit cell design as shown in Figure 5, the S-parameters were measured across a frequency range centered around 17 GHz which are represented in Figure 6. These parameters help determine how the metasurface interacts with incident electromagnetic waves — specifically, whether it reflects or transmits them. The electromagnetic response of the metasurface varies with frequency, revealing key performance characteristics such as resonance behaviour and absorption.

In the simulation setup, the design was configured using a 2×2 array in the pattern tool. Appropriate boundary conditions were defined to accurately model the periodic behaviour and ensure the reliable extraction of the scattering parameters (S_{11}, S_{21}, etc.)

Set the simulation conditions by applying appropriate boundary settings and utilising a Floquet port to excite the structure. Perform the simulation in the frequency domain, and define field monitors specifically at 17 GHz to capture the necessary field distributions. Monitor the S-parameters, particularly S_{11} and S_{21}, to analyze the reflective and cross-polarised responses. These parameters are essential for evaluating the metasurface's behaviour within the Ku-band (12–18 GHz), especially for applications involving stealth technology.

3.2. 4×4 CSAD Metasurface

Finally, construct a $4 * 4$ metasurface unit cell design shown in Figure 6, where the periodicity of unit cell increases, then the proposed design will perform more accurately.

The unit cell must be arranged periodically to produce a 4×4 array, like a far-field radiation pattern, RCS, or coupling analysis.

The ***S*-parameters** must be calculated, and responses for a 4×4 array are as shown in Figure 11. To analyze the results, the unit cell will be kept under a waveguide, i.e., vector analyzer as shown in Figure 7.

4. ABSORPTION OF CSAD

The absorbance of a metasurface unit cell can be calculated for the proposed design, in which it can achieve high absorption over the Ku band for frequency ranges, often exceeding 90% as shown in Figure 8. The high absorbance can be obtained by varying the CSAD's geometry, structure, and material properties. The absorbance is calculated using the formula $A = 1 - R_a - T_a$, where $R_a = |S_{11}|^2$ and $T_{\mathrm{a}} = |S_{21}|^2$ are the reflectance and transmittance derived from the S-parameter, respectively. The function of the metasurface unit cell is absorptance (A) [25], and it can be calculated using a mathematical expression

$$A = 1 - |S_{11}|^2 - |S_{21}|^2 \tag{7}$$

Since there is no transmission at S_{21}, i.e., $S_{21} = 0$, absorbance expression becomes

$$A = 1 - |S_{11}|^2 \tag{8}$$

5. PARAMETRIC ANALYSIS OF THE PROPOSED ABSORBER

A parametric analysis is performed to assess how parameters affect the design performance, length, width, and angle of the design, also the effect of incidence angle θ and polarization. The S-parameter and absorptivity can be observed by modifying the length and width of the design L_s as shown in Figures 9(a) and (b).

The observed S-parameters and absorption are represented in Table 1. As parameter L_s increases, the reflection coefficient decreases at $L_s = 10.375$ mm, and its reflection is -35.4 dB, indicating optimum impedance matching with free space. Also, absorbance is improved from 96% to 99%, and higher increases in L_s generate mild detuning, resulting in a minor loss in reflection performance, as illustrated in Table 2.

6. ANGULAR STABILITY

Angular stability measures how well the metasurface absorber maintains its absorption performance as the incident angle (Θ) increases. The suggested geometry is analyzed for polarization angles $\phi = 0°, 20°, 40°$, and $60°$, and the corresponding ab-

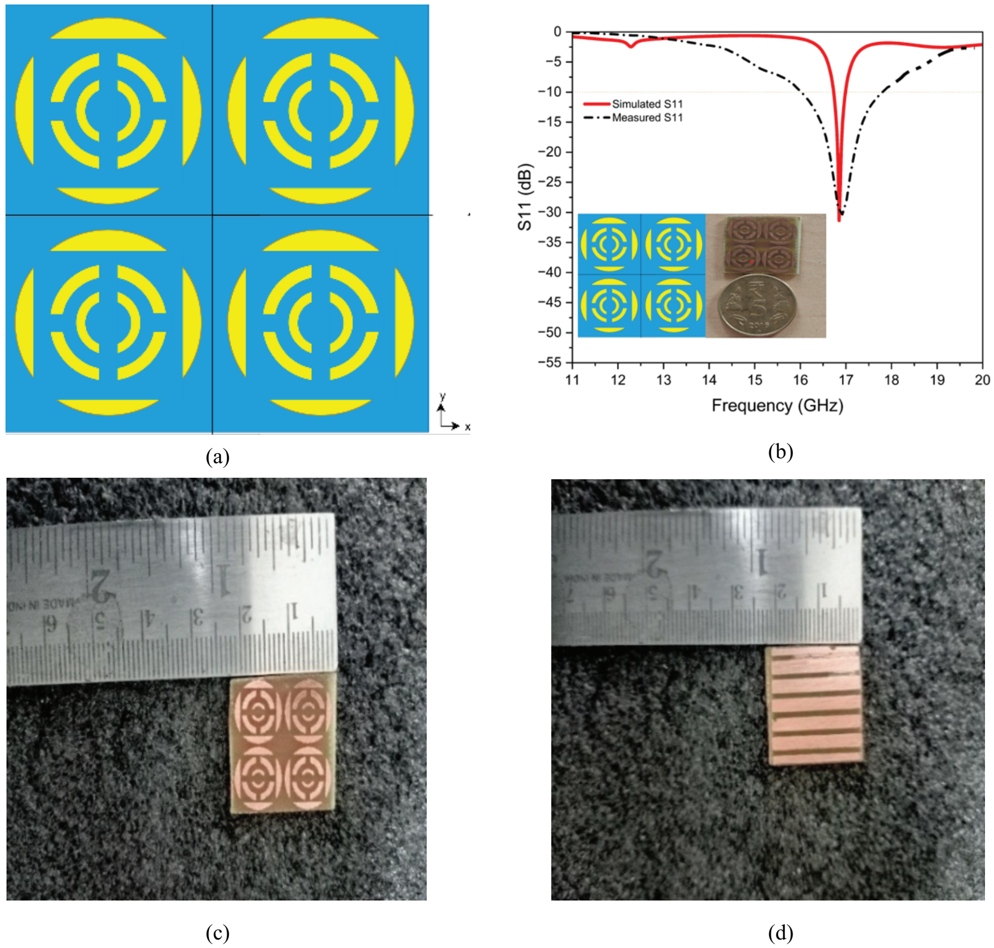

FIGURE 5. (a) Front view of 2×2 simulated CSAD metasurface, (b) Frequency response for 2×2 CSAD, (c) & (d) Front & back views of the fabricated 2×2 metasurface.

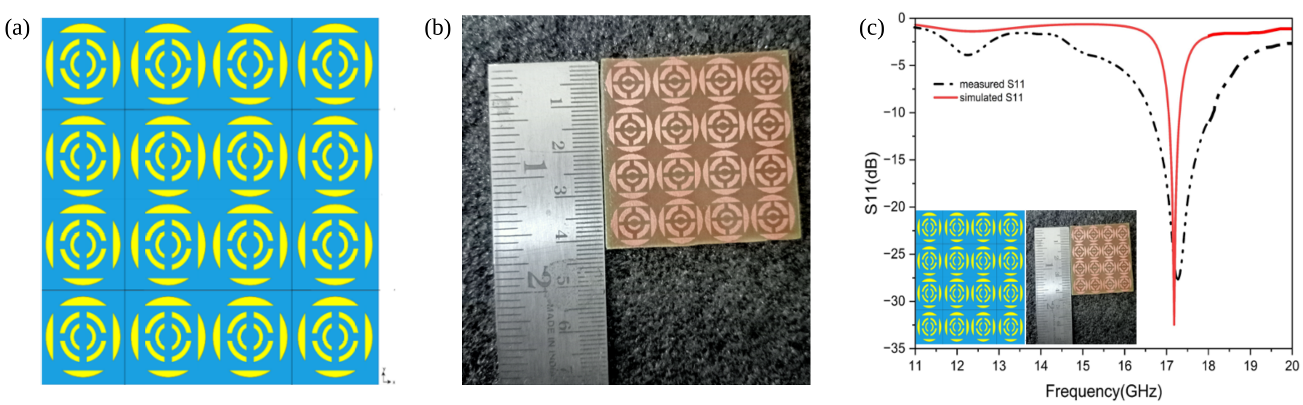

FIGURE 6. 4×4 simulated metasurface, (b) Fabricated metasurface, (c) Frequency response of 4×4 metasurface.

sorption characteristics are observed under oblique incidence. A highly angularly-stable absorber has high absorption with very little resonance shift for oblique incidence angles up to 60° for both TE and TM polarizations..

TE and TM modes: This research explores the polarisation stability of the proposed unitcell configuration via both transverse electric (TE) and transverse magnetic (TM) analysis, as shown in Figures 10(a) and 10(b). Moreover, owing to the geometric configuration and symmetry, both TE and TM polarisations exhibit significant angular stability. For TE polarisation, incidence angles of 0°, 20°, 40°, and 60° yield S_{11} values exceeding -15 dB across the frequency band, as demonstrated in Figure 10(a). Figure 10(b) indicates that the stopband surpasses the resonant stopbands by more than -15 dB.

FIGURE 7. Fabricated 4×4 metasurface with measured results.

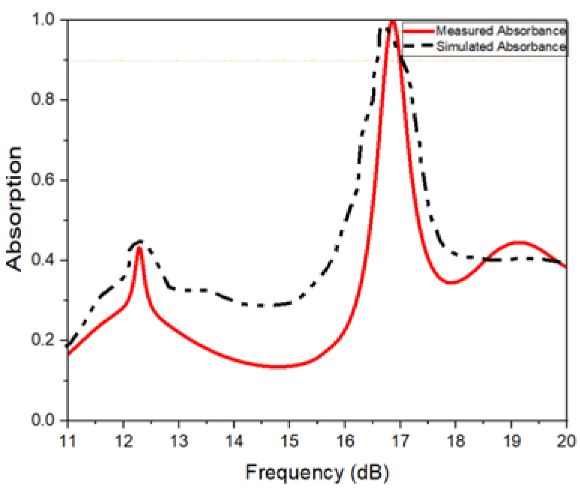

FIGURE 8. Absorbance for simulated and measured results of CSAD-based metasurface.

Additionally, the bandwidth ratio approaches unity for both bands, signifying enhanced angular stability. Figure 10(b) presents the simulated and measured S_{11} magnitude curves for TM polarisation. When an electromagnetic wave strikes the absorber at an oblique incidence angle of 60°, the TE and TM modes reveal unique responses in the electric (E) field with the surface configuration, as represented in Figure 10.

Polarization sensitivity of CSAD is defined by the dependence of its absorption characteristics on the incident wave polarization. A polarization-independent CSAD metasurface exhibits identical absorption under TE and TM excitations, whereas a polarization-sensitive design shows distinct TE/TM responses and is analyzed through TE and TM simulations at incidence angles of 0°, 20°, 40°, and 60°.

TABLE 2. Observations in parametric analysis of L_s from 10.125 to 10.5 mm.

Variation in size L_s (mm)	Resonating Frequency (GHz)	Reflection value (dB)	Absorbance (%)
10.125	17.426	−14.5	96
10.25	17.273	−20.1	99
10.375	17.12	−35.4	99
10.5	16.8	−30.6	99

7. *E*-FIELD AND SURFACE CURRENT DISTRIBUTIONS

The surface distribution of the electric (E) and magnetic (H) fields in a metasurface design operating in the Ku-band at 17 GHz is crucial for understanding the behaviour of electromagnetic waves represented in Figure 11. Observations of the E and H field distributions indicate strong localized fields at the operating frequency, confirming that the metasurface functions effectively as an absorptance (A).

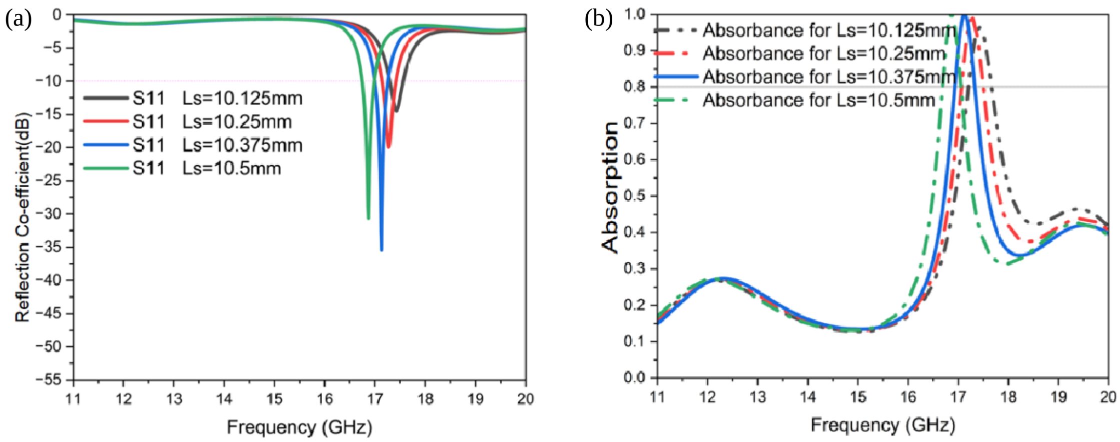

FIGURE 9. Parametric analysis of L_s from 10.125 to 10.5 mm.

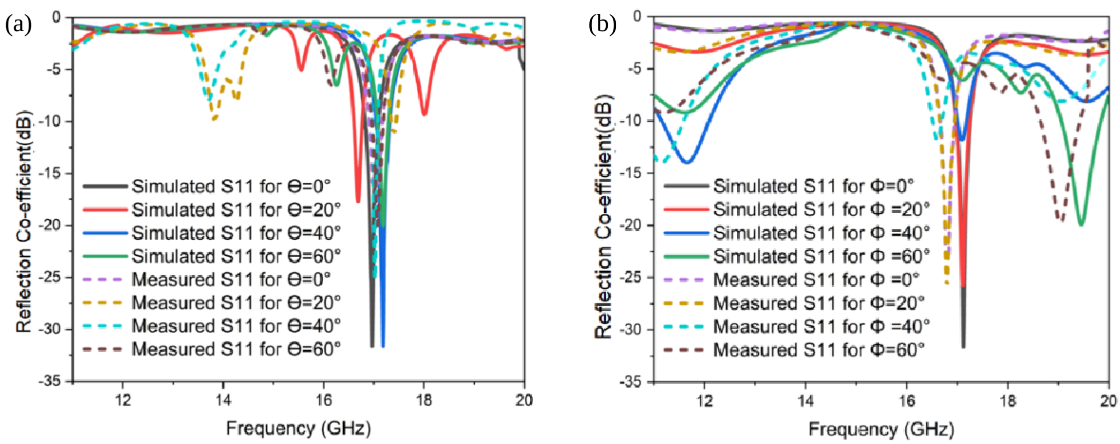

FIGURE 10. S_{11}-parameters with polarization angles of Θ and ϕ variation.

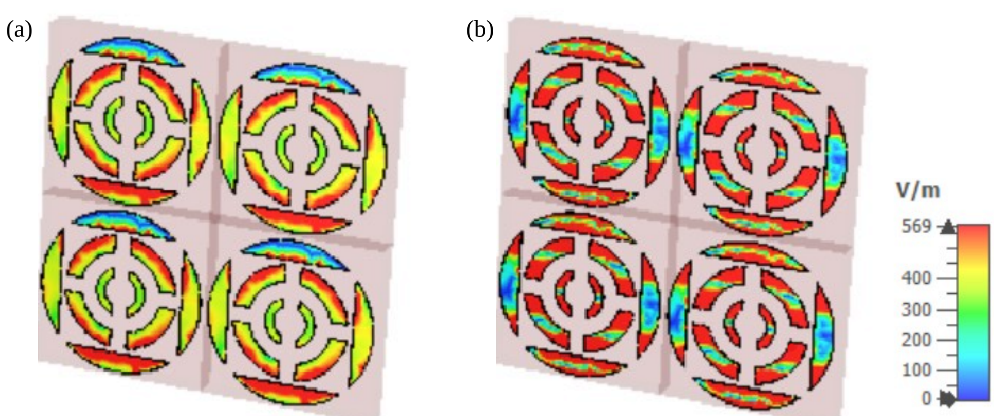

FIGURE 11. (a) E field at 17 GHz frequency. (b) E field at 17.2 GHz frequency.

8. RADAR CROSS-SECTION (RCS) REDUCTION

Radar Cross-Section (RCS) reduction in metasurface unit cells is a critical area of research aimed at enhancing stealth technology by minimizing the detectability of objects by radar systems at frequencies 17 GHz to 17.2 GHz. Additionally, the field behaviour suggests a reduced RCS, further validating the design's potential for stealth applications. From Figure 12, it can be observed that the longer slots are responsible for the lower resonating bands, and the shorter slots are responsible for the higher resonating bands. Various strategies have been

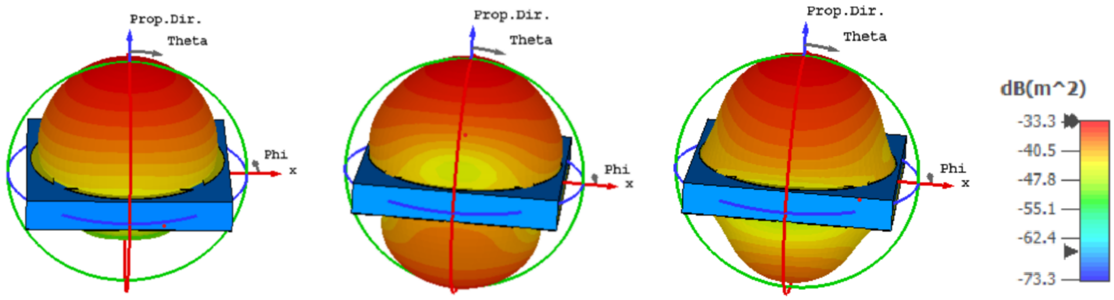

FIGURE 12. Far-field RCS at 17 GHz, 17.1 GHz, 17.2 GHz.

TABLE 3. Comparison between proposed CSAD and previous designs.

Ref	Physical Size of Unit cell	Dielectric constant (ε_r)/ Thickness [mm]	Band edges	Bandwidth	Angle for oblique incidence/ Angle vs Response	RCS reduction	Absorption
[19]	$14 \times 14\,\text{mm}^2$	$4.3/0.8$	5.68 GHz & 8.75 GHz	0.6 GHz & 0.45 GHz	60°	yes	$> 90\%$
[29]	$5.5 \times 5.5\,\text{mm}^2$	4.3/0.02	28.9 GHz to 31.9 GHz	3 GHz	20°	No	$> 90\%$
[30]	$10 \times 10\,\text{mm}^2$	2.17/0.0009	8.86 GHz and 8.848 GHz	0.74 GHz	0° to 60°	No	$> 90\%$
[31]	$18 \times 18\,\text{mm}^2$	4.3/0.02	3.88 GHz	0.326 GHz	20°	yes	$> 80\%$
[32]	$14 \times 14\,\text{mm}^2$	2.1/0.07	8 GHz and 10 GHz	2 GHz	60°	High	$= 90\%$
[33]	$50 \times 50\,\text{nm}^2$	not explicitly stated	8 GHz and 10 GHz	1 GHz	20°	no	$> 90\%$
Proposed work	$10.375\times 10.375\,\text{mm}^2$	4.3/0.02	16.9 GHz and 17.2 GHz	0.3 GHz	60°	yes	99.9%

developed to achieve effective RCS reduction through innovative metasurface designs and configurations. These approaches typically involve novel unit cell geometries, which collectively contribute to scattering suppression and reduced radar signature.

9. COMPARING PROPOSED CSAD WITH PREVIOUS DESIGNS

Compared to earlier designs, the proposed metasurface absorber outperforms them as shown in Table 3. With a tiny unit-cell dimension of $10.375 \times 10.375\,\text{mm}^2$, a dielectric constant of 4.3, and a thickness of 0.02 mm, it achieves a narrow band absorption from 17.0 GHz to 17.2 GHz. The structure exhibits strong angular stability up to 60° for both TE and TM polarisations, with absorption efficiency reaching 99%.

The primary objective is to make the Unmanned Aerial Vehicle (UAV) less conspicuous to radar systems that function at or near 17 GHz. Absorbing the impinging electromagnetic waves at 17 GHz frequency effectively attenuates the UAV's signature on radar displays. At 17 GHz, it retains significant relevance for satellite detection and various military applications. These enhancements provide excellent impedance matching, robust loss characteristics, and consistent performance, making the suggested design uses for stealth applications.

10. CONCLUSION

In this paper, a CSAD-based metasurface is presented that is applicable to electromagnetic wave shielding in defence applications. The proposed unit cell features two dipoles integrated with a symmetric Split Ring Resonator (SRR) on a substrate with a dielectric constant of 4.3 and a loss tangent of 0.02. The design resonates at 17 GHz with a bandwidth of 300 MHz, angular stability at 60°, and 99.9% absorption. The unit cell size for the proposed design is $10.375 \times 10.375 \times 1.6\,\text{mm}^2$. The metasurface significantly reduces RCS, demonstrating its potential for stealth applications. For unmanned aerial vehicles, the proposed metasurface array can be engineered to selectively absorb radar signals at 17 GHz. This design can be effectively applied to reduce radar visibility in platforms such as stealth aircraft, naval ships, submarines, missiles, and unmanned aerial vehicles (UAVs). The proposed design's validity is supported by findings obtained from both simulated and measured data collected from the prototype.

REFERENCES

[1] Yogeshwaran, A. and K. Umadevi, "An efficient wideband low noise amplifier (WLNA) using advanced design system based industrial micro strip antenna," *Microprocessors and Microsystems*, Vol. 79, 103302, 2020.

[2] Hu, J., S. Bandyopadhyay, Y.-H. Liu, and L.-Y. Shao, "A review on metasurface: From principle to smart metadevices," *Frontiers in Physics*, Vol. 8, 586087, 2021.

[3] Budhu, J., N. Ventresca, and A. Grbic, "Unit cell design for aperiodic metasurfaces," *IEEE Transactions on Antennas and Propagation*, Vol. 71, No. 9, 7387–7394, 2023.

[4] Anitha, C., V. Singh, A. K. Dwivedi, and N. K. Narayanaswamy, "Review: Metamaterial/metasurface applications in antenna domain," *Opto-Electronics Review*, Vol. 32, No. 3, e151692, 2024.

[5] Li, A., S. Singh, and D. Sievenpiper, "Metasurfaces and their applications," *Nanophotonics*, Vol. 7, No. 6, 989–1011, 2018.

[6] Khan, B., B. Kamal, S. Ullah, I. Khan, J. A. Shah, and J. Chen, "Design and experimental analysis of dual-band polarization converting metasurface for microwave applications," *Scientific Reports*, Vol. 10, No. 1, 15393, 2020.

[7] Qi, Y., B. Zhang, C. Liu, and X. Deng, "Ultra-broadband polarization conversion meta-surface and its application in polarization converter and RCS reduction," *IEEE Access*, Vol. 8, 116 675–116 684, 2020.

[8] Budhu, J., N. Ventresca, and A. Grbic, "Unit cell design for aperiodic metasurfaces," *IEEE Transactions on Antennas and Propagation*, Vol. 71, No. 9, 7387–7394, 2023.

[9] Fadhil, T. Z., N. A. Murad, M. K. A. Rahim, M. R. Hamid, and L. O. Nur, "A beam-split metasurface antenna for 5G applications," *IEEE Access*, Vol. 10, 1162–1174, 2021.

[10] Geng, W., Q. Guo, J. Su, and Z. Li, "Dartboard metasurface for RCS reduction and OAM wave generation," *IEEE Transactions on Antennas and Propagation*, Vol. 73, No. 4, 2497–2509, 2025.

[11] Bandyopadhyay, B., S. Bhattacharya, R. K. Jaiswal, M. Saikia, and K. V. Srivastava, "Wideband RCS reduction of a linear patch antenna array using AMC metasurface for stealth applications," *IEEE Access*, Vol. 11, 127 458–127 467, 2023.

[12] Song, Z., J. Zhu, L. Yang, P. Min, and F. H. Lin, "Wideband metasurface absorber (metabsorber) using characteristic mode analysis," *Optics Express*, Vol. 29, No. 22, 35 387–35 399, 2021.

[13] Saxena, G., S. Kumar, S. Chintakindi, A. Al-Tamim, M. H. Abidi, W. A. M. Saif, S. Kansal, R. Jain, S. Singh, A. K. Dohare, P. K. Maduri, M. Kumar, H. Singh, and Y. K. Awasthi, "Metasurface instrumented high gain and low RCS X-band circularly polarized MIMO antenna for IoT over satellite application," *IEEE Transactions on Instrumentation and Measurement*, Vol. 72, 1–10, 2023.

[14] Koohestani, M. and A. Ghaneizadeh, "An ultra-thin double-functional metasurface patch antenna for UHF RFID applications," *Scientific Reports*, Vol. 11, No. 1, 857, 2021.

[15] Coelho, H. J. S., B. Araújo, M. W. B. Silva, T. N. Ferreira, A. L. P. S. Campos, C. Junqueira, E. Kemptner, and A. Osipov, "Multiband metasurface-based absorber for applications in X, Ku, and K bands," *Radio Science*, Vol. 58, No. 8, 1–11, 2023.

[16] Zhang, L., C. Gao, H. Guo, H. Zhang, Z. Zhao, and T. Liu, "Efficient polarization conversion metasurface for scattered beam control and RCS reduction," *Scientific Reports*, Vol. 14, No. 1, 26260, 2024.

[17] Gu, H., "Antenna stealth design based on polarization reconfigurable metasurfaces," in *2024 IEEE 7th International Conference on Electronic Information and Communication Technology (ICEICT)*, 322–326, Xi'an, China, 2024.

[18] Joy, V., A. Dileep, P. V. Abhilash, R. U. Nair, and H. Singh, "Metasurfaces for stealth applications: A comprehensive review," *Journal of Electronic Materials*, Vol. 50, No. 6, 3129–3148, 2021.

[19] Shao, L. and W. Zhu, "Recent advances in electromagnetic metamaterials and metasurfaces for polarization manipulation," *Journal of Physics D: Applied Physics*, Vol. 57, No. 34, 343001, 2024.

[20] Solunke, Y. and A. Kothari, "A low-RCS dual-bandstop golden ratio-based fractal-FSS for defense applications," *International Journal of Communication Systems*, Vol. 38, No. 4, e5997, 2025.

[21] Younis, F., O. Khan, J. Ahmad, M. J. Qasim, H. Luo, and S. Wang, "A highly efficient triple band metasurface enabled absorber for 5G/6G millimeter wave applications," *Scientific Reports*, Vol. 15, No. 1, 29455, 2025.

[22] Nipun, M. M. K., M. J. Islam, and M. Moniruzzaman, "A triple-band metamaterial absorber for gas sensing and refractive index detection through enhanced FOM and Q-factor performance in the THz regime," *Results in Optics*, Vol. 21, 100822, 2025.

[23] Faysal, M., M. T. Islam, M. K. Uddin, M. L. Hakim, B. Bais, K. Mat, and A. F. Almutairi, "Polarization independent interconnected split-ring resonator with enclosed F shape metamaterial absorber for wireless technology," in *2024 International Conference on Electromagnetics in Advanced Applications (ICEAA)*, 627–635, Lisbon, Portugal, September 2024.

[24] Huang, Q., W. Xie, F. Z. Alqahtany, T. Cao, G. A. M. Mersal, and Z. Toktarbay, "Study on thin-layer broadband metamaterial absorber based on composite multi-opening ring pattern of magnetic dielectric layers," *Advanced Composites and Hybrid Materials*, Vol. 8, No. 2, 180, 2025.

[25] Hasan, M. M., M. T. Islam, M. Salaheldeen, S. H. A. Almalki, A. G. Alharbi, H. Alsaif, M. S. Islam, and M. Samsuzzaman, "Polarization insensitive dual band metamaterial with absorptance for 5G sub-6 GHz applications," *Scientific Reports*, Vol. 12, No. 1, 8495, 2022.

[26] Chen, X., T. M. Grzegorczyk, B.-I. Wu, J. Pacheco, Jr., and J. A. Kong, "Robust method to retrieve the constitutive effective parameters of metamaterials," *Physical Review E*, Vol. 70, No. 1, 016608, 2004.

[27] Tsang, L. and J. A. Kong, *Scattering of Electromagnetic Waves: Advanced Topics*, John Wiley & Sons, 2004.

[28] Moss, C. D., T. M. Grzegorczyk, Y. Zhang, and J. A. Kong, "Numerical studies of left handed metamaterials," *Progress In Electromagnetics Research*, Vol. 35, 315–334, 2002.

[29] Singh, V., S. Bhattacharyya, and R. Agrahari, "A low-profile tri-functional metasurface toward polarization conversions and absorption," *IEEE Antennas and Wireless Propagation Letters*, Vol. 23, No. 9, 2593–2597, 2024.

[30] Bakir, M., K. Delihacioglu, M. Karaaslan, F. Dincer, and C. Sabah, "U-shaped frequency selective surfaces for single-and dual-band applications together with absorber and sensor configurations," *IET Microwaves, Antennas & Propagation*, Vol. 10, No. 3, 293–300, 2016.

[31] Jasim, M. B. and K. Sayidmarie, "Radar cross-section reduction of planar absorbers using resistive FSS unit cells," *Journal of Telecommunications and Information Technology*, No. 4, 61–67, 2023.

[32] Yadav, J., M. Saikia, K. V. Srivastava, and J. Ramkumar, "Three-dimensional rotation of FSS unit cell in broadband microwave absorber for large oblique incidence response," *IEEE Transactions on Electromagnetic Compatibility*, Vol. 65, No. 5, 1320–1328, 2023.

[33] Azad, A. K., W. J. M. Kort-Kamp, M. Sykora, N. R. Weisse-Bernstein, T. S. Luk, A. J. Taylor, D. A. R. Dalvit, and H.-T. Chen, "Metasurface broadband solar absorber," *Scientific Reports*, Vol. 6, No. 1, 20347, 2016.